Segmentation and filtering of tubular structures in 2D and 3D

Hugues Talbot, Odyssée Merveille, Nicolas Passat, Laurent Najman

Institut Pascal 2019 October 14

UNIVERSITÉ PARIS-EST

Gaspard - Monge - Laboratoire d'informatique

Outline

The Vivabrain project

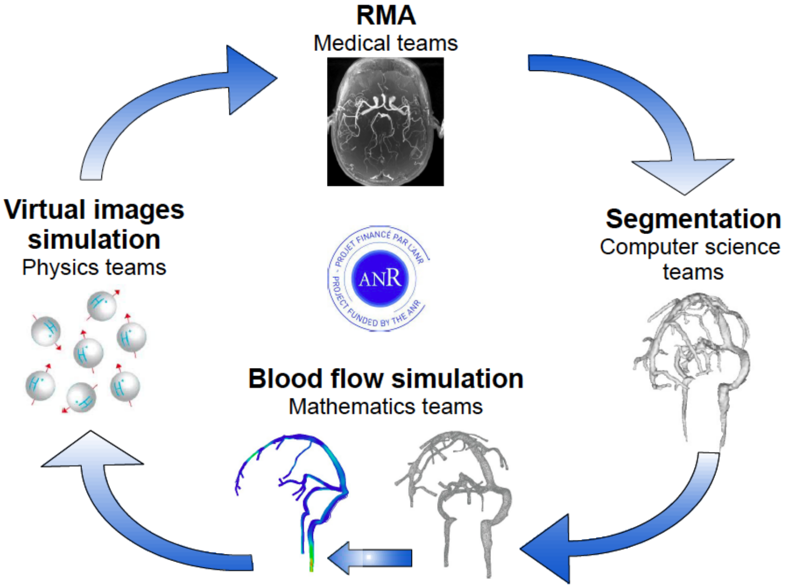

Step 1: Extracting the vascular network from brain MRA data

- **Filtering**
  Improve images (Denoising, contrast enhancement)
- **Segmentation**
  Detecting the vascular network
- **Post-processing**
  Reconnexion, quantitative data analysis: directions, diameter, vessel density ...)

Classical approach for tubular segmentation

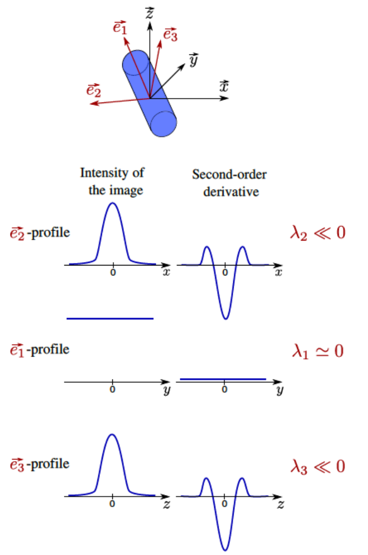

Figure: Classical approach using the Hessian

Problems with local scale-space derivatives

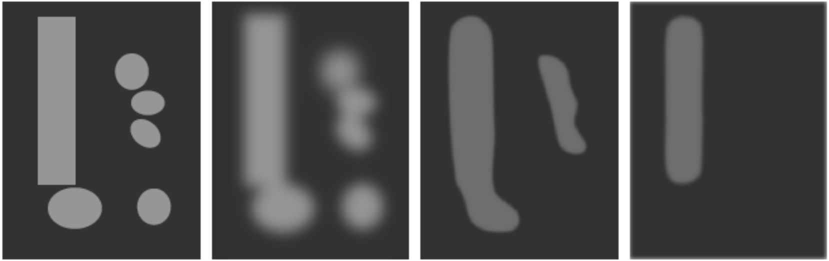

(a) Initial image (b) Gaussian filter result (c) Hessian-based filter result (d) Expected result

Figure: Scale-space locality problem

Errors in estimation due to locality

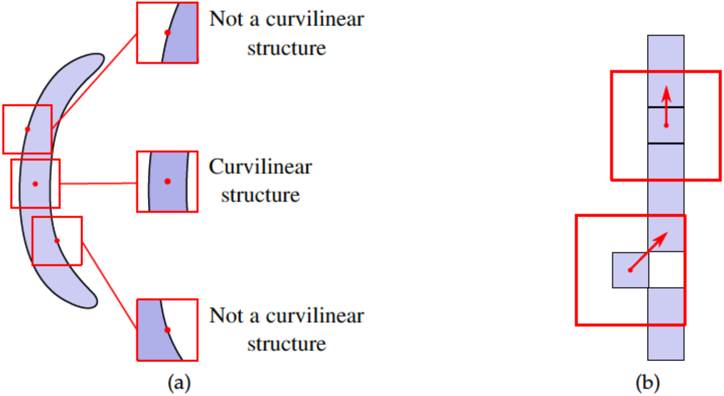

Figure: Errors due to locality

In this talk

A new filtering method to improve existing segmentation pipeline

2 complementary axes :

- Noise reduction
- Vascular network contrast enhancement

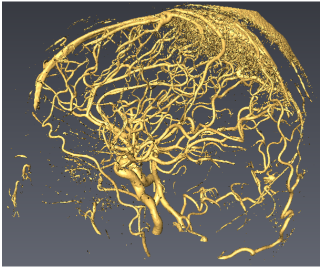

3D MRA data surface rendering

Maximum intensity projection

Adjacency graph

A path, **a**, is a set of neighboring pixels on a graph defining an adjacency relation $x \to y$:

$$\mathbf{a} = (a_1, a_2, ..., a_L) \quad si \;\; a_k \to a_{k+1}$$

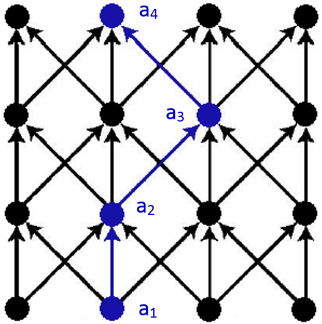

Adjacency graph (black)
*and vertical path **a** of length 4 (blue).*

Filtering of an image by a path opening

Preserving thin structures in arbitrary orientations imposes to filter the image by several paths each using a particular adjacency graph.

The 2D space is discretized in 4 different orientations :

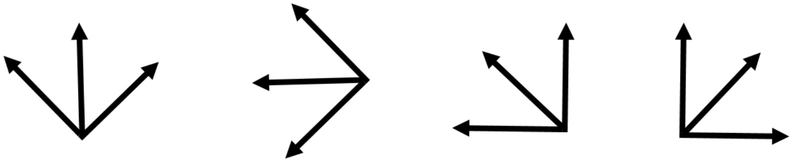

Multiple orientations in 3D

In 3D, the discrete space is discretized in 7 different orientations :

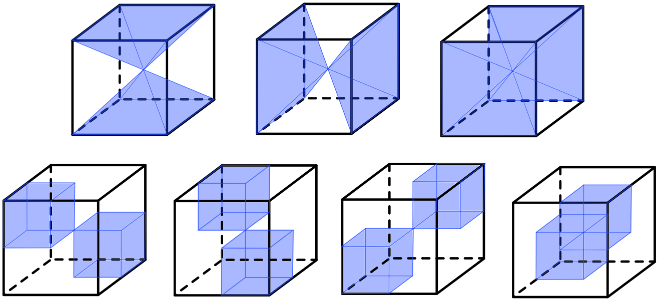

Path filtering

Example binary path opening

$$\alpha_L = \bigvee \{\sigma(\mathbf{a}), \mathbf{a} \in \Pi_L(X)\}$$

σ_L : Set of all pixels belonging to path **a**.
$\Pi_L(X)$: Set of all paths of length L.

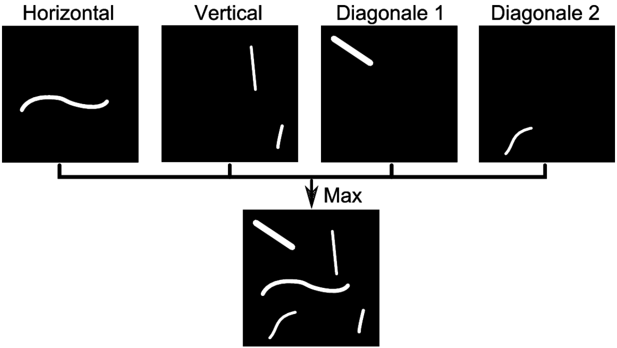

Principle

Path definition relaxation

A path can now admit K consecutive noise pixels between path pixels

This makes it possible to preserve partially disconnected thin/tubular structures :

Path with $L = 10$ *and* $K = 1$ *noise pixel*

This notion is different from that of *path incompleteness* by Heijman et al, it was proposed by F. Cokelaer [Cok13] and is simpler to implement.

Example

RPO Example on a synthetic, noisy 2D image (AWGN mean $= 0, \sigma = 20$
:

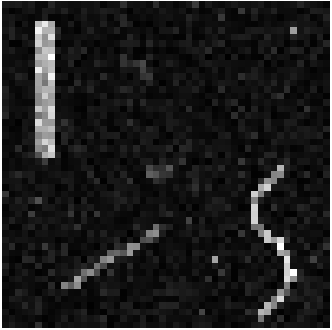

Initial image 50x50px

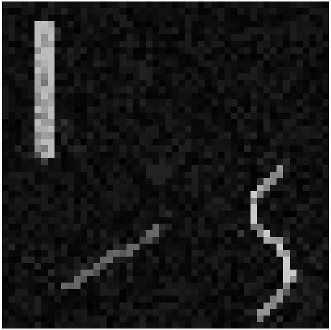

RPO L=10, K=1

The 3D case is more complicated than 2D

2D Case

2 Types of structures :

Fibres and Blobs

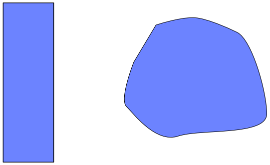

RPO preserves only fibres if blobs are not too big.

3D Case

3 types de structures :

Tubes, Planes and Blobs

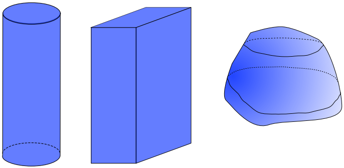

RPO preserves both tubes and planes.

An RPO by itself preserves more than just tubes in 3D images. Another filter is thus necessary to eliminate planar structures.

Principle

Hypothesis

Planar structures should be detected in at least one more orientation than tubular structures

Test of this hypothesis on 3 synthetic structures :

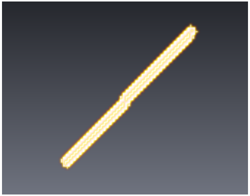

Tube

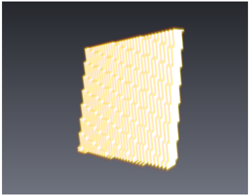

Plane

Half-ellipsoid surface

Hypothesis testing

Test :

Filtering 100 3D images of each structure and measuring the number of RPO orientations still containing the structure after filtering

Histogram of the number of orientations preserving the synthetic structure:

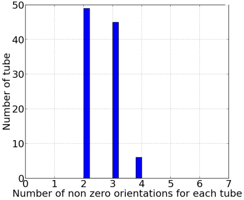

Tubes

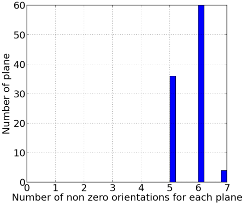

Planes

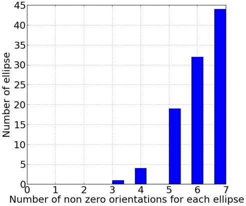

Half-ellipsoids

New operator

We order the result of each RPO orientation pixelwise and compute

$$\text{RORPO} = RPO_1 - RPO_i$$

RPO_1 : Result of standard RPO (max of all RPOs)
RPO_i : The $i-th$ rank of the RPO.

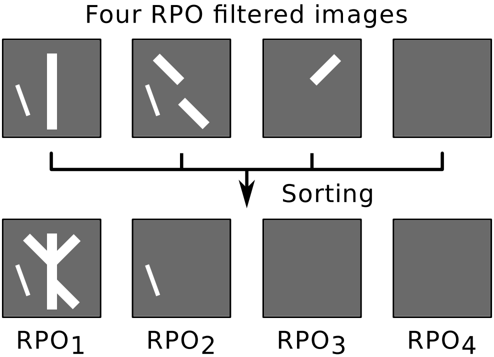

Robustness test

We compute the RORPO error rate on 100 random synthetic structure of each type.

$$\%error = \frac{nb_{error}}{nb_{pixels}} \times 100$$

nb_{error}: number of false negative pixels for the tubes and of false positifs for the planes and half-ellipsoids.

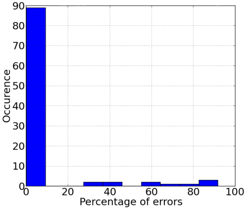

Tubes $(m = 4\%)$

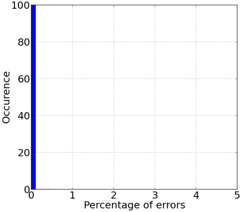

Planes $(m = 0\%)$

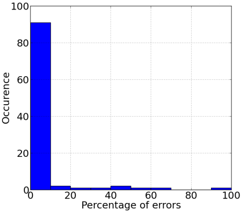

Half ellipsoids $(m = 4\%)$

What is a multi-scale approach ?

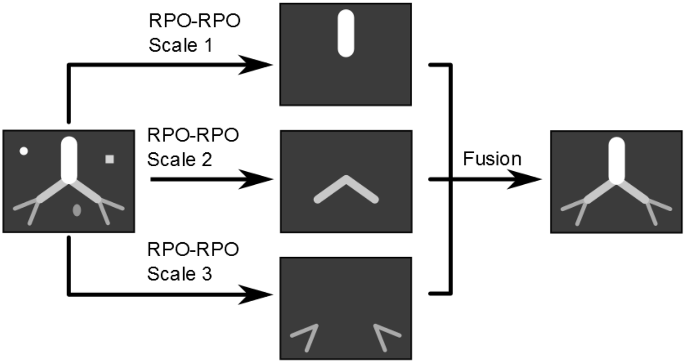

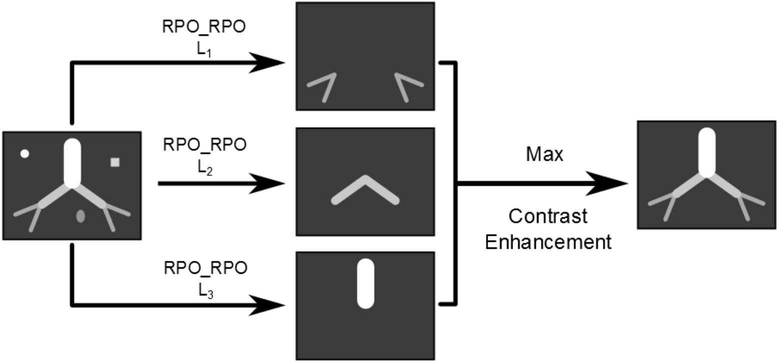
RPO_RPO
L1
RPO_RPO
L2
RPO_RPO
L3
Max
Contrast
Enhancement

Intensity result in 2D

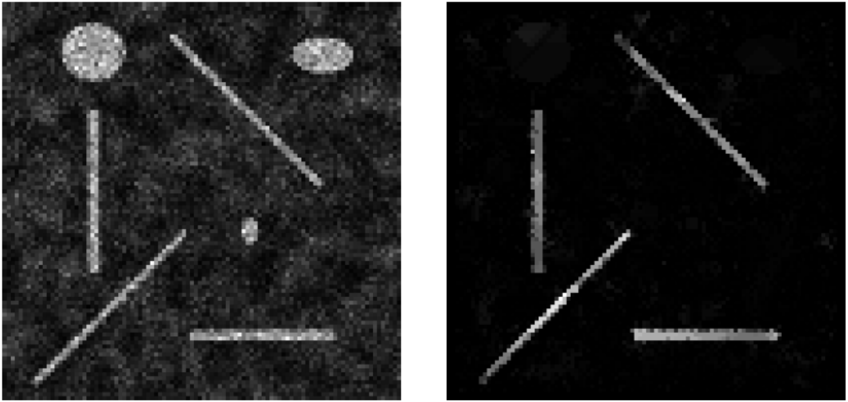

(a) Initial image (b) the RORPO intensity result

Figure: Intensity feature in 2D

Intensity result in 3D on a real MRA

Initial image

RORPO with a multiscale approach

Orientation result in 2D

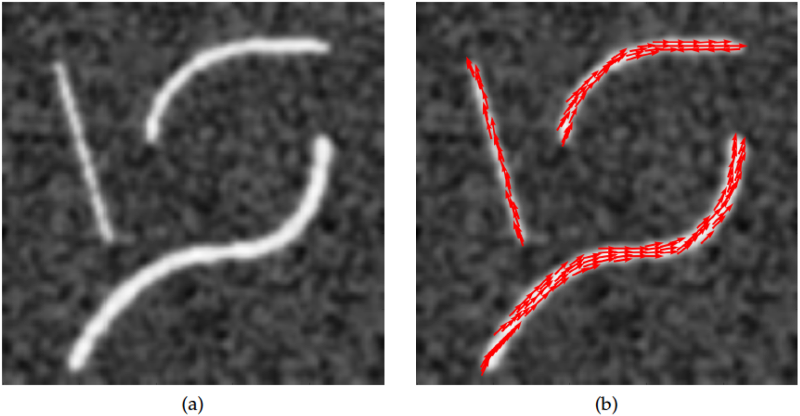

Figure: Orientation feature in 2D

Comparisons

We performed qualitative comparisons of various methods according to four criteria on a full cerebral MRA

- Capacity to reduce background noise
- Capacity to detect large blood vessels
- Capacity to detect small blood vessels
- Presence of artifacts

RORPO with classical adjacencies and a multiscale approach based on path lengths seems to provide the best compromise.

Quantitative comparison

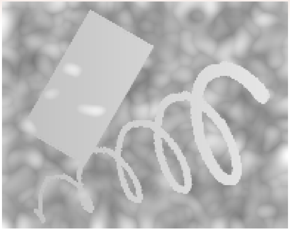

(a) CCM=0.605, Dice=0.634

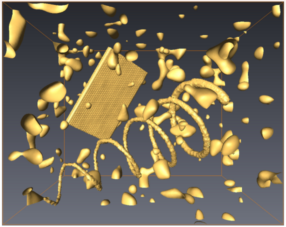

(b)

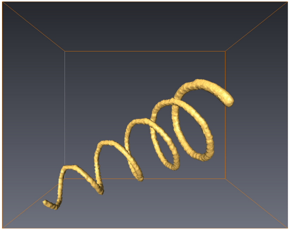

(c)

Figure: Synthetic image: (a) maximum intensity projection and (b) isosurface. (c) Ground truth.

Quantitative comparison - filtering result

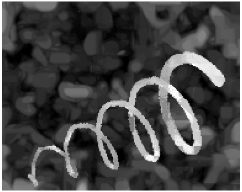

(a) CCM=0.884, Dice=0.893

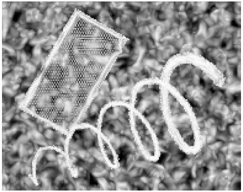

(b) CCM=0.706, Dice=0.730

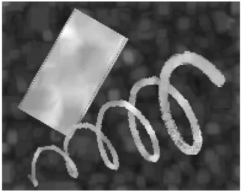

(c) CCM=0.655, Dice=0.654

Figure: Filtered synthetic image: maximum intensity projection. (a) RORPO. (b) Frangi's vesselness. (c) and RPO-top-hat.

Quantitative comparison - ROC analysis

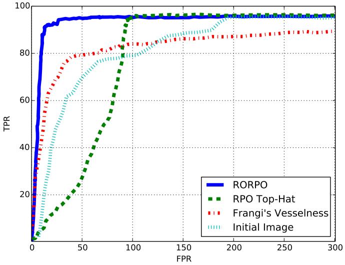

(a)

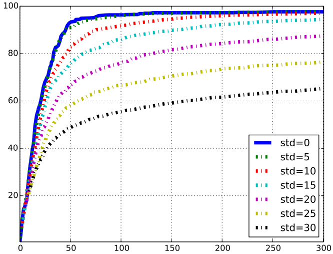

(b)

Figure: ROC curves on synthetic data. (a) Comparison of the three filters, plus the native image. (b) Noise robustness of the RORPO filter.

Quantitative comparison, synthetic data

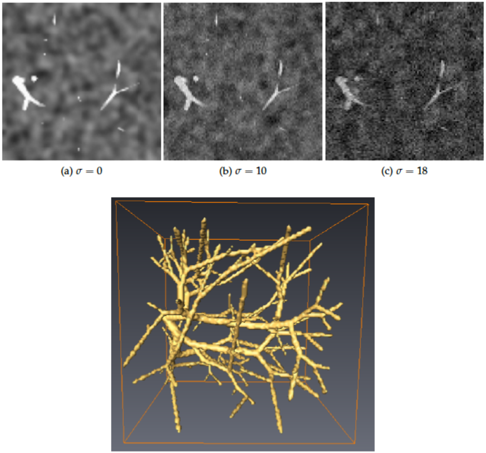

(a) $\sigma = 0$ (b) $\sigma = 10$ (c) $\sigma = 18$

(d)

Figure: Synthetic 3D data

Quantitative comparison, synthetic data, ROC analysis

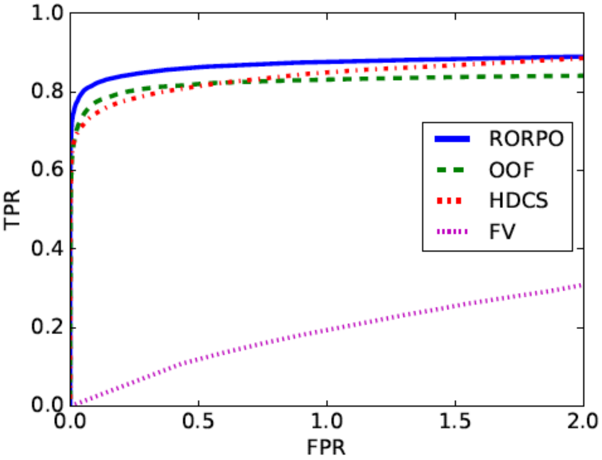

Figure: Three-way ROC analysis

MRA result

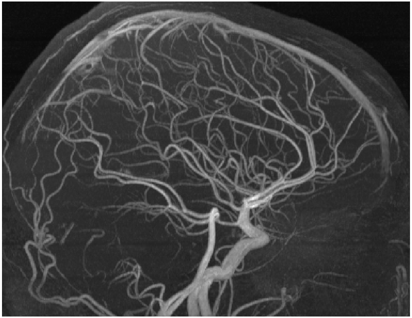

Initial image MIP

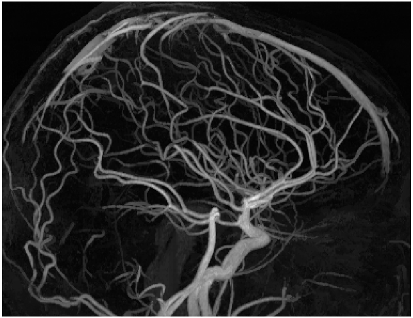

RORPO with a length-based multiscale approach

Quantitative comparison on HF data

(a)

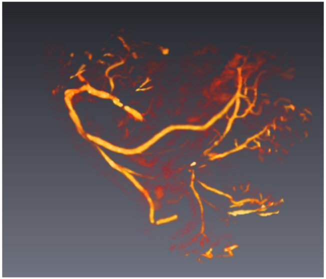

(b) MCC = 0.541

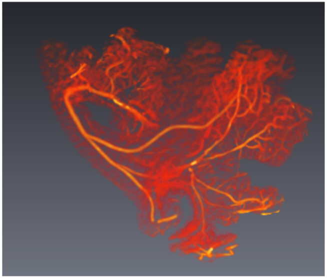

(c) MCC = 0.529

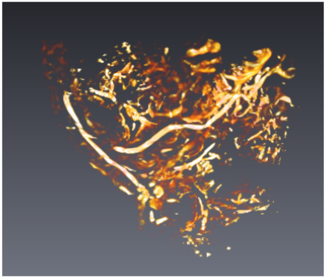

(d) MCC = 0.405

Comparaison with Frangi vesselness

Proposed method isosurface

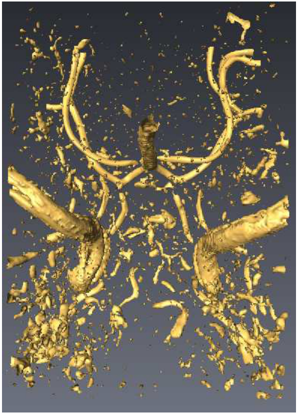

Optimized Frangi vesselness isosurface

Quantitative comparison - MICCAI Rotterdam Coronaries Database

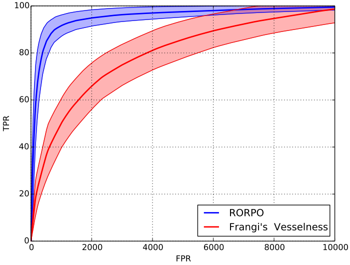

Figure: ROC curves of RORPO and Frangi's Vesselness on the Rotterdam repository. For both filtering the central curve is the mean ROC curve and the two others are the mean plus or minus one standard deviation ROC curve.

Orientation feature 3D

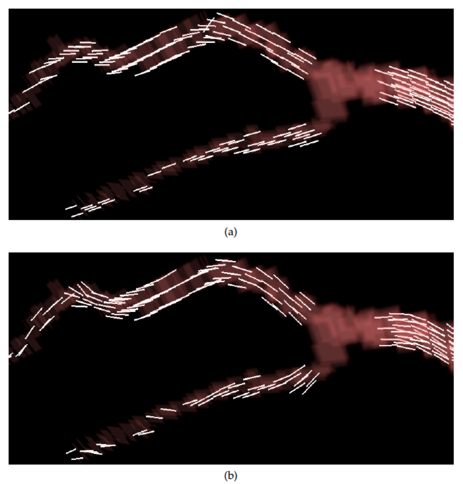

Figure: Orientation feature in 3D, HF data: RORPO (a) vs FV (b)

Optimization approach

Model

$$\underset{x}{\text{minimize}} \max_{\|F\|_\infty \leq 1} F^\top((Ax)\sqrt{w}) + \frac{1}{2\lambda}\|x - f\|^2 \qquad (1)$$

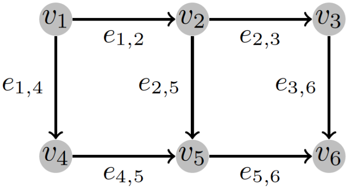

$$A = \begin{array}{c|cccccc|}
 & v_1 & v_2 & v_3 & v_4 & v_5 & v_6 \\
\hline
e_{1,2} & -1 & 1 & 0 & 0 & 0 & 0 \\
e_{2,3} & 0 & -1 & 1 & 0 & 0 & 0 \\
e_{4,5} & 0 & 0 & 0 & -1 & 1 & 0 \\
e_{5,6} & 0 & 0 & 0 & 0 & -1 & 1 \\
e_{1,4} & -1 & 0 & 0 & 1 & 0 & 0 \\
e_{2,5} & 0 & -1 & 0 & 0 & 1 & 0 \\
e_{3,6} & 0 & 0 & -1 & 0 & 0 & 1
\end{array}$$

FIG. 1.1. *A graph and its incidence matrix* $A \in \mathbb{R}^{m \times n}$ *with* $m = 7$ *and* $n = 6$.

Directional TV idea

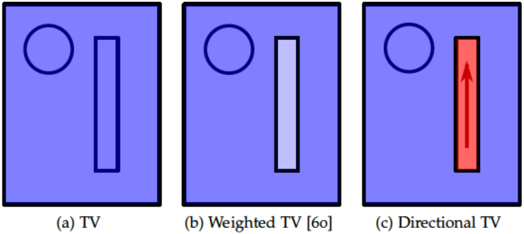

Figure: Directional TV idea

Discrete Span

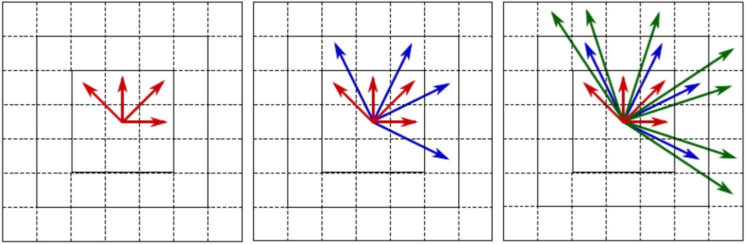

(a) $n = 1$ (b) $n = 2$ (c) $n = 3$

Figure: Vector span

Directional TV theoretical edge weight

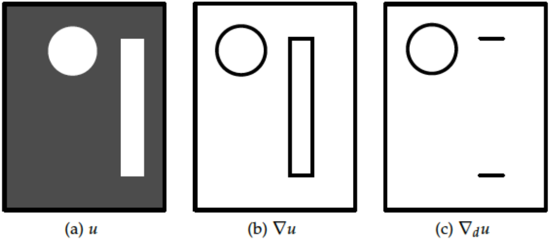

Figure: Theoretical edge weights

DRIVE result

(a) Background corrected initial image

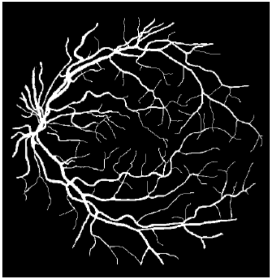

(b) Ground truth

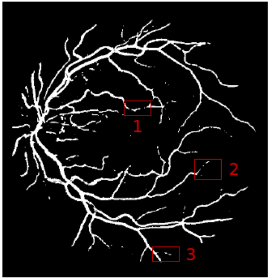

(c) Chan model

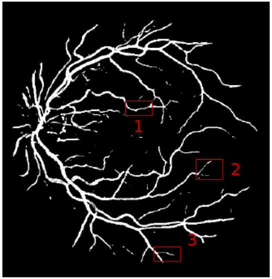

(d) Proposed model

DRIVE result details

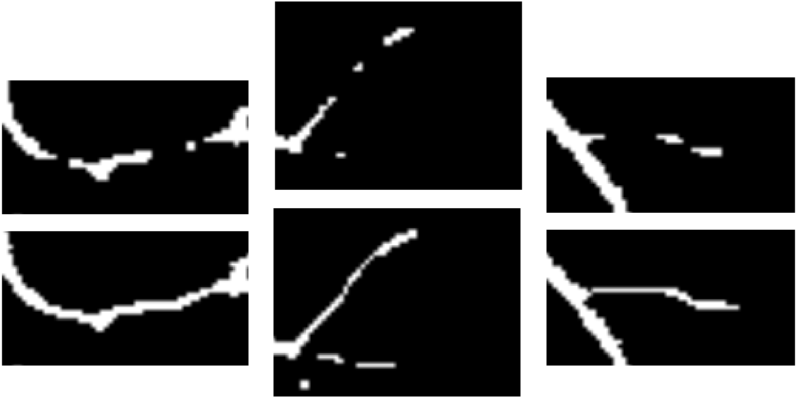

(e) box 1 (f) box 2 (g) box 3

Figure: 2D Result on DRIVE (details)

Primal-dual algorithm for solving this model

Let $\gamma \in (0, +\infty)$, $u_0 \in \mathbb{R}^N$ and $u_1 \in \mathbb{R}^N$.
Set $x_0 \in \mathbb{R}^N$, and $\forall r \in \{0, \ldots, R\}$, $v_{r,0} \in \mathbb{R}^{P_r}$.
For $k = 0, \ldots$

$$
\left\lfloor
\begin{array}{l}
y_{1,k} = x_k - \gamma \left(\nabla \varphi(x_k) + \sum_{r=0}^{R} V_r^\top v_{r,k} \right) \\
p_{1,k} = \mathrm{prox}_{\gamma \iota_{\mathcal{X}}}(y_{1,k}) \\
\text{For } r = 0, \ldots, R \\
\left\lfloor
\begin{array}{l}
y_{2,r,k} = v_{r,k} + \gamma V_r x_k \\
p_{2,r,k} = \mathrm{prox}_{\gamma \psi_r^*}(y_{2,r,k}) \\
q_{2,r,k} = p_{2,r,k} + \gamma V_r p_{1,k} \\
v_{r,k+1} = v_{r,k} - y_{2,r,k} + q_{2,r,k}
\end{array}
\right. \\
q_{1,k} = p_{1,k} - \gamma \left(\nabla \varphi(p_{1,k}) + \sum_{r=0}^{R} V_r^\top p_{2,r,k} \right) \\
x_{k+1} = x_k - y_{1,k} + q_{1,k}
\end{array}
\right.
$$

Results 3D

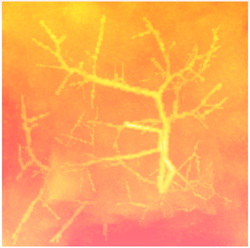

(a) Original (max. projection view)

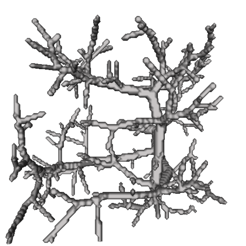

(b) Ground truth

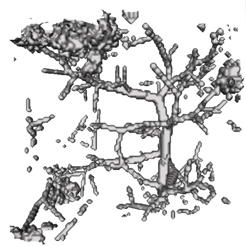

(c) Piecewise const. (0.753, 0.984)

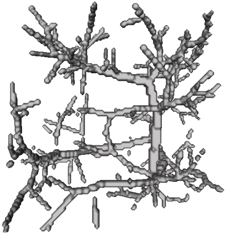

(d) Ours (0.835, 1.000)

Restoration 3D, with Poisson noise

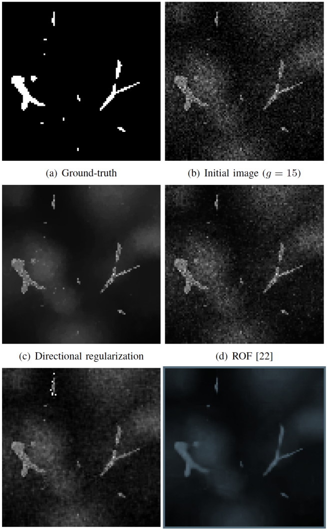

(a) Ground-truth
(b) Initial image ($g = 15$)
(c) Directional regularization
(d) ROF [22]
(e) HDCS [46]
(f) BM4D [40]

Figure: Restoration with mixed gradient: slices

Restoration 3D, with Poisson noise

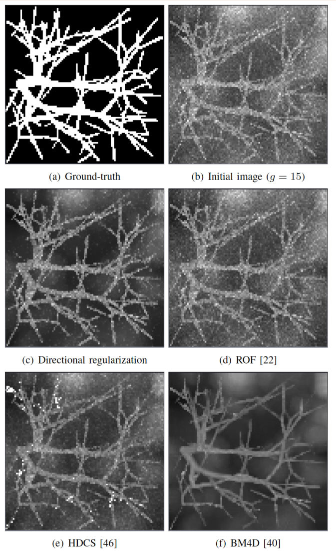

Figure: Restoration with mixed gradient: Max Intensity Projections

Restoration 3D, with Poisson noise

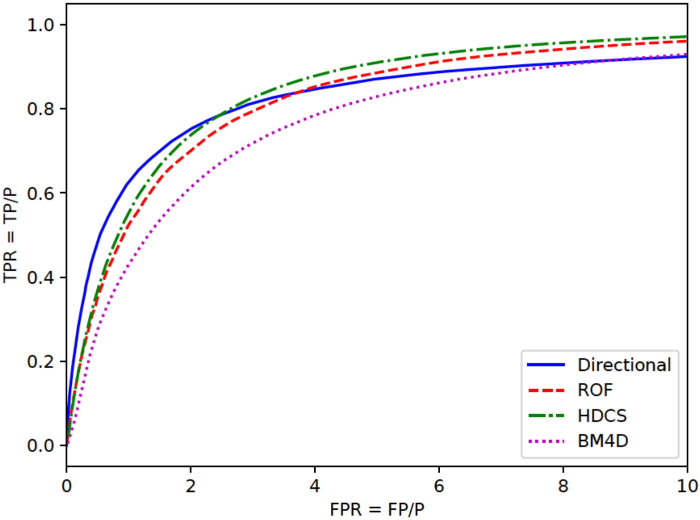

Figure: Restoration with mixed gradient: Max Intensity Projections

Conclusion

We have studied three thin object filtering methods :

- *RPO_Opening*
- RORPO
- RORPO with restricted adjacencies

Associated with two multiscale approaches :

- Based on path length
- Based on path diameters

The best compromise was found to be RORPO with classical adjacencies and length-based multiscale approach. Our method is effective at

significantly reducing background noise while simultaneously reducing non-tubular structures and preserving the majority of blood vessels.

Current work

Quantitative evaluation of our results :

- Use ground truth from MICCAI & Heartflow Inc MRA data.
- Applications in small veins detection in the human brain with NIH and Max-Planck institute: link with multiple sclerosis.
- Application to angio CT of the small animal.

Perspectives

- Produce images of scales
- Adapt the path operator framework to the max-tree/min-tree framework
  - This would allow discriminating objects on more complex measures than mere length
  - Think about incorporating robustness to max-trees / min-trees

Literature on path operators

- Definitions and early algorithms [BT00, HBT04, HBT05]
- Faster algorithms [AT05, TA07]
- Extension to 3D and regularisation [LH10]
- RPO and 3D [Cok13], [CTC12]
- RORPO, segmentation, restoration [MTNP14, MTNP15, MNT+17, MTNP18, MNTP18]
- Applications [VCBT09, VCB+09, VCB+10, SVB+14]
- DCTV [CGN+13]

Thanks for your attention

References I

- Ben Appleton and Hugues Talbot, *Efficient path openings and closings*, Mathematical Morphology: 40 Years On (Dordrecht) (C. Ronse, L. Najman, and E. Decencière, eds.), Computational Imaging and Vision, vol. 30, Springer-Verlag, 2005, pp. 33–42.
- M. Buckley and H. Talbot, *Flexible linear openings and closings*, Mathematical Morphology and its application to image analysis (Palo Alto), Kluwer, June 2000, pp. 109–118.
- C. Couprie, L. Grady, L. Najman, J.-C. Pesquet, and H. Talbot, *Dual constrained TV-based regularization on graphs*, SIAM Journal on Imaging Sciences **6** (2013), no. 3, 1246–1273.
- François Cokelaer, *Améliorations des ouvertures par chemins pour l'analyse d'images à n dimensions et implémentations optimisées*, Ph.D. thesis, Université de Grenoble, 2013.
- F. Cokelaer, H. Talbot, and J. Chanussot, *Efficient robust d-dimensional path operators*, IEEE Journal of Selected Topics in Signal Processing **6** (2012), no. 7, 830 –839.

References II

H. Heijmans, M. Buckley, and H. Talbot, *Path-based morphological openings*, Proceedings of IEEE ICIP 2004 (Singapore), October 2004, pp. 3085–3088.

——, *Path openings and closings*, Journal of Mathematical Imaging and Vision **22** (2005), 107–119.

C.L. Luengo Hendriks, *Constrained and dimensionality-independent path openings*, Image Processing, IEEE Transactions on **19** (2010), no. 6, 1587–1595.

Odyssée Merveille, Benoît Naegel, Hugues Talbot, Laurent Najman, and Nicolas Passat, *2d filtering of curvilinear structures by ranking the orientation responses of path operators (rorpo)*, Image Processing On Line **7** (2017), 246–261.

Odyssée Merveille, Benoît Naegel, Hugues Talbot, and Nicolas Passat, *nD variational restoration of curvilinear structures with directional regularization*, working paper or preprint, July 2018.

References III

Odyssee Merveille, Hugues Talbot, Laurent Najman, and Nicolas Passat, *Tubular structure filtering by ranking orientation responses of path operators*, Computer Vision–ECCV 2014, Springer, 2014, pp. 203–218.

Odyssée Merveille, Hugues Talbot, Laurent Najman, and Nicolas Passat, *Ranking orientation responses of path operators: Motivations, choices and algorithmics*, International Symposium on Mathematical Morphology and Its Applications to Signal and Image Processing, Springer, 2015, pp. 633–644.

O. Merveille, H. Talbot, L. Najman, and N. Passat, *Curvilinear structure analysis by ranking the orientation responses of path operators*, IEEE Transactions on Pattern Analysis and Machine Intelligence **40** (2018), no. 2, 304–317.

References IV

Eysteinn Már Sigurdsson, Silvia Valero, Jon Atli Benediktsson, Jocelyn Chanussot, Hugues Talbot, and Einar Stefánsson, *Automatic retinal vessel extraction based on directional mathematical morphology and fuzzy classification*, Pattern Recognition Letters **47** (2014), 164–171.

H. Talbot and B. Appleton, *Efficient complete and incomplete paths openings and closings*, Image and Vision Computing **25** (2007), no. 4, 416–425.

S. Valero, J. Chanussot, J.A. Benediktsson, H. Talbot, and B. Waske, *Directional mathematical morphology for the detection of the road network in very high resolution remote sensing images*, Proceedings of ICIP 2009 (Cairo, Egypt), 2009, pp. 3725–3728.

———, *Advanced directional mathematical morphology for the detection of the road network in very high resolution images*, Pattern Recognition Letters **31** (2010), no. 10, 1120–1127.

References V

S. Valero, J. Chanussot, J.A. Benediktsson, and H. Talbot, *Détection automatique du réseau vasculaire rétinien basée sur la morphologie directionnelle et la fusion de décision*, Proceedings of GRETSI (Dijon, France), INIST-CNRS, 2009, Paru.